J Nanopart Res (2012) 14:706
DOI 10.1007/s11051-011-0706-3

RESEARCH PAPER

Controlled synthesis and magnetic properties of nickel phosphide and bimetallic iron–nickel phosphide nanorods

Bhupendra Singh · Chia-Ling Ho · Yuan-Chieh Tseng · Chieh-Tsung Lo

Received: 17 August 2011 / Accepted: 26 December 2011 / Published online: 25 January 2012

Abstract Nickel phosphide (Ni_2P) and bimetallic iron–nickel phosphides [$(Fe_xNi_y)_2P$] nanorods were fabricated by a seeded growth strategy. This strategy utilized pre-synthesized Fe_3O_4 nanoparticles as seeds and the thermal decomposition of metal precursors by multiple injections in a solution containing trioctylphosphine and didodecyldimethylammonium bromide (DDAB). The nanorods were characterized by transmission electron microscopy, X-ray diffraction, and magnetic measurements were carried out using superconducting quantum interference device (SQUID). The rod length was tunable, ranging from 10 to 110 nm depending on the number of injections, whereas the diameter of the rods was nearly 6 nm. It was found that the rod size increased with the number of injections under the constant total injection concentration and reaction time. In addition, the effect of the DDAB quantity used as a co-surfactant was studied, which showed that an optimum quantity was required to achieve uniform nanorods. Magnetic characterizations were performed over the two kinds of nanorods to identify their respective magnetic phases. The results demonstrated that the Ni_2P nanorods were defined as a Curie–Weiss paramagnet, whereas the $(Fe_xNi_y)_2P$ nanorods exhibited superparamagnetic characteristics.

Keywords Nickel phosphide · Nanorods · Multiple injections · Magnetic property

B. Singh · C.-L. Ho · C.-T. Lo (✉)
Department of Chemical Engineering, National Cheng Kung University, No. 1, University Road, Tainan City 70101, Taiwan, ROC
e-mail: tsunglo@mail.ncku.edu.tw

Y.-C. Tseng
Department of Materials Science & Engineering, National Chiao Tung University, 1001 Ta Hsueh Road, Hsin-Chu 30010, Taiwan, ROC

Introduction

One-dimension (1D) nanostructured materials including nanorods, nanowires, nanotubes, and nanocables, of transition metals have attracted great research interests due to their novel properties arising from their shape anisotropy and their potential applications in magnetic storage media, anode materials, molecular separation, catalysts, biomedical applications, etc. (Bai et al. 2004; Chubykalo-Fesenko and Chantrell 2004; Boyanov et al. 2006; Lee et al. 2004; Senevirathne et al. 2007; Liu et al. 2006). Therefore, the recent progress in the synthesis and characterization of 1D materials has been mainly driven by the need to understand their physico-chemical properties in a variety of novel nanoscale devices. Metal-rich Ni_2Ps such as Ni_2P, Ni_3P, Ni_5P_2, and Ni_6P_5 that form a large family of useful materials are all very important. They have attracted considerable interests due to their excellent properties and potential applications, such as catalytic, corrosion-resistant, oxidation-resistant,

and wearproof materials (Bieger 1997; Sawhill et al. 2003; Oyama 2003; Motojima et al. 1979; Zhang et al. 2010; Wang and Smith 2010; Motojima et al. 1981). Because of the special structure of di-nickel phosphide nanocrystallites, they are also promising candidates for luminescent devices, magnetic, or electronic components (van Schnering and Honle 1994).

Several synthesis routes have been reported for transition metal phosphides in literature, such as reaction of a gaseous mixture at high temperature (Motojima et al. 1979), hydrogen plasma reduction of oxidic precursors (Wang et al. 2008; Guan et al. 2009), solvothermal method (Qian et al. 1998; Yunle et al. 2002), surfactant-added solvothermal route (Liu et al. 2003), arrested precipitation reactions with organometallic precursors (Brock et al. 2004), supported synthesis by impregnation (Sawhill et al. 2003; Wang et al. 2002), thermolysis of the single-source (Lukehart et al. 1998), and a mild route employing reactions of nickel chloride and sodium hypophosphite at low temperatures (Xie et al. 2005). Recently some attempts have been made for the phase controlled synthesis of transition metal phosphide nanoparticles (Muthuswamy et al. 2009; Wang et al. 2010a, b). For example, Wang et al. (2010a, b) proposed an Ullmann-type reaction approach for phase-controllable synthesis of transition metal phosphide nanostructures by reactions of transition metal powders with triphenylphosphine in vacuum-sealed tubes.

Many attempts have also been made to synthesize 1D transition metal phosphides (Gregg et al. 2006; Lo and Kuo 2010). Qian et al. (2004) prepared well-defined FeP nanorods and nanowires by multiple injections of iron pentacarbonyl and phosphine mixtures in a surfactant-assisted synthesis. Park et al. presented a generalized synthesis route for uniform sized transition metal phosphide nanorods from the thermal decomposition of continuously delivered metal–phosphine complex using a syringe pump (Park et al. 2004; Park et al. 2005; Yoon et al. 2008). According to them, the use of a syringe pump is necessary to get 1D metal phosphide nanostructures and they controlled the diameters and aspect ratios of the nanorods by tuning the injection rate along with various surfactants. However, later studies have shown that 1D metal phosphide nanostructures can also be prepared by multiple manual injections of metal–phosphine complex as opposed to the continuous injection of complex using a syringe pump (Hou et al. 2004; Kelly et al. 2007; Wang et al. 2010a, b).

We recently fabricated iron phosphide nanorods by multiple injections of $Fe(CO)_5$ in a solution containing trioctylphosphine (TOP), didodecyldimethylammonium bromide (DDAB), and pre-synthesized magnetite nanoparticles (Lo and Kuo 2010). Unlike other one-step thermal decomposition or multiple injection methods to produce metal phosphide nanorods, we synthesized nanorods by first preparing nucleation seeds. The injection of stock solution comprising metal precursor and surfactants induced oriented attachments of particles, leading to the growth of nanorods directly on the nucleation seeds. In this method, the pre-synthesized magnetite nanoparticles appeared to act as a template for the growth of nanorods, and the diameter of nanorods remains nearly identical to that of the magnetite nanoparticles. In this finding, the length of the nanorods is tunable to the number of injections, as well as the concentrations of the injection components. Herein, we have employed a simple, whereas novel route, as combining a seed-template and the thermal decomposition method for the synthesis of Ni_2P and bimetallic $(Fe_xNi_y)_2P$ nanorods. The synthesized nanorods were then characterized by magnetic measurements. We demonstrate that a fair control over the structural configuration and magnetic properties is feasible using the proposed strategy.

Experimental section

Sample preparation

Due to the hazardous nature of $Fe(CO)_5$, it was stored in a refrigerator maintained at −20 °C prior to use. In addition, all the manipulations were performed using standard air-free techniques. The procedure for the synthesis of spherical iron particle seeds was presented elsewhere (Peng et al. 1998; Park et al. 2000). Briefly, 1.0 g of $Fe(CO)_5$ (97%, Sigma-Aldrich Co.) and 3.0 g of trioctylphosphine oxide (TOPO, 99%, Sigma-Aldrich Co.) were mixed at 70 °C to form $Fe(CO)_5$–TOPO mixture. The resulting mixture was added immediately into the preheated TOPO (10.0 g) at 340 °C under an argon atmosphere and aged for 30 min at 320 °C. The as-synthesized nanoparticles were purified by the addition of excess acetone to remove the residual ions and TOPO. These nanoparticles were re-dispersed in 10 mL of pyridine and used as nucleation seeds for rod formation.

The procedure to prepare Ni_2P nanorods was a modification of the method reported for the synthesis of Fe_2P nanorods in our earlier work (Lo and Kuo 2010). Briefly, a stock solution of $Ni(acac)_2$–TOP mixture was prepared by mixing $Ni(acac)_2$ and TOP with the proportions as described in Table 1. 5.0 g of TOP (90%, Sigma-Aldrich Co.) and 0.5 g of DDAB (98%, Sigma-Aldrich Co.) were mixed with 1.5 mL pyridine-dispersed solution of pre-synthesized magnetite nanoparticles. This mixture was heated to 320 °C under an argon atmosphere. The stock solution of $Ni(acac)_2$–TOP was manually injected via a syringe into the mixture at different time intervals as described in Table 1 while maintaining the reaction mixture at 320 °C for 180 min. During this period, the thermal decomposition of $Ni(acac)_2$–TOP took place, leading to anisotropic growth along the seed particles and resulting in rod-shaped Ni_2P nanoparticles. To obtain the relationship between the number of injections and the size of nanorods, we varied the injection condition to control the length of these rods.

To understand the effect of DDAB quantity on the nanorod synthesis, Ni_2P nanorods were synthesized by varying the DDAB quantity from 0.15, 0.50, 0.75 to 1.0 g while keeping other parameters constant as described in Table 1 for 8 injections at 320 °C for 180 min. After the completion of reaction, the resulting rods were washed with *n*-hexane and subsequently collected by centrifugation five times. Finally, the rods were dried in a vacuum oven at 50 °C and were kept for further characterizations.

For the synthesis of bimetallic iron–nickel phosphide nanorods with different compositions, we followed the compositions mentioned by Yoon et al. (2008). The compositions of various reactants and the reaction parameters are given in Tables 2 and 3. Briefly, 5.0 g TOP and 0.5 g DDAB were mixed with 1.5 mL pyridine-dispersed solution of pre-synthesized magnetite nanoparticles. This mixture was heated to 320 °C under an argon atmosphere. The stock solutions of $Ni(acac)_2$–TOP and $Fe(CO)_5$–TOP were separately prepared by mixing $Ni(acac)_2$ and $Fe(CO)_5$ with TOP in the proportions as described in Table 2 and 3. The stock solutions were manually injected via a syringe into the mixture at different time intervals while maintaining the reaction mixture at 320 °C for 3 h. After the completion of reaction, the resulting rods were washed with *n*-hexane and subsequently collected by centrifugation five times. Finally, the rods were dried in a vacuum oven at 50 °C and were kept for further characterizations.

Table 1 Composition of the reactants for the synthesis of Ni_2P nanorods by varying the number of injections of $Ni(acac)_2$–TOP to Fe_3O_4 seeds

Number of injections	Amount of $Ni(acac)_2$ per injection (mg)	Total amount of $Ni(acac)_2$ injected (mg)	Amount of TOP per injection (g)	Total amount of TOP injected (g)	Time between successive injections (min)
6	30	180	1.20	7.2	30
8	22.5	180	0.90	7.2	22.5
12	15	180	0.60	7.2	15
15	12	180	0.48	7.2	12

The total reaction time was 180 min

Table 2 Composition of the reactants for the synthesis of $(Fe_xNi_y)_2P$ nanorods with 6 injections of $Ni(acac)_2$–TOP to Fe_3O_4 seeds

Composition of nanorods	$Fe(CO)_5$ + TOP (mg/injection)	$Ni(acac)_2$ + TOP (mg/injection)	Total amount of $Ni(acac)_2$ injected (mg)	Time between successive injections (min)
$(Fe_{0.90}Ni_{0.10})_2P$	75 + 500	8.4 + 700	50	30
$(Fe_{0.80}Ni_{0.20})_2P$	75 + 500	25.0 + 700	150	30
$(Fe_{0.75}Ni_{0.25})_2P$	75 + 500	41.7 + 700	250	30

Total amount of $Fe(CO)_5$ injected was 450 mg and the total reaction time was 180 min

Table 3 Composition of the reactants for the synthesis of $(Fe_{0.80}Ni_{0.20})_2P$ nanorods by varying the number of injections of $Fe(CO)_5$–TOP and $Ni(acac)_2$–TOP to Fe_3O_4 seeds

Number of injections	$Fe(CO)_5$ + TOP (mg/injection)	$Ni(acac)_2$ + TOP (mg/injection)	Time between successive injections (min)
6	75.00 + 500	25.00 + 700	30
8	56.25 + 375	18.75 + 525	22.5
12	37.50 + 250	12.50 + 350	15

The total reaction time was 180 min

Characterization of nanorods

The length and diameter of magnetic nanorods were characterized by transmission electron microscopy (TEM), operated on a Hitachi H7500 electron microscope. Samples for TEM analysis were prepared by making a drop of particle solution on a copper grid coated with a carbon film. X-ray diffraction (XRD) patterns were obtained using a Rigaku RINT-2000 diffractometer. Data were collected with an angle-dependent scan from 20° to 80° with a scan rate of 5°/min. The magnetic measurements of the nanorods were performed using a superconducting quantum interference device (SQUID, MPMS XL-7) at National Sun Yat-Sen University in Taiwan. Temperature-dependent magnetization measurements were carried out in a temperature range from 10 to 300 K with field-cooled (FC) and zero-field-cooled (ZFC) conditions, where the field strength of the condition was 100 Oe.

Results and discussion

Synthesis of magnetic spherical particles

Figure 1a shows TEM image of the spherical nanoparticles used as the nucleation seeds for the preparation of nickel phosphide nanorods. The diameter of the seed nanoparticles was 5.5 ± 1.2 nm. In Fig. 1b, the XRD pattern reveals that these particles can be indexed as Fe_3O_4 structure (JCPDS Card No. 89-0691), regardless of the weak peak intensities resulted from the nanostructure.

Synthesis of nanorods

In this study, the synthesis of Ni_2P and $(Fe_xNi_y)_2P$ nanorods with different aspect ratios was achieved by the use of multiple injections of precursor materials. Conventional studies employed a syringe pump for the continuous delivery of precursor to induce the growth of nanorods (Liu et al. 2006; Bieger 1997; Sawhill et al. 2003; Muthuswamy et al. 2009; Wang et al. 2010a, b; Gregg et al. 2006). Unlike this conventional approach, we injected the same total amount of precursor into the mixture of the nucleation seeds and surfactants, but varied the number of injections. Figure 2 shows the TEM of the Ni_2P nanorods as a function of the number of injections, for which the detailed experimental conditions are shown in Table 1. In these reactions, the total amount of injected $Ni(acac)_2$ and TOP, and the total reaction time were kept constant. It was observed that both the length and the aspect ratio of the Ni_2P nanorods were highly dependent on the number of injections. The

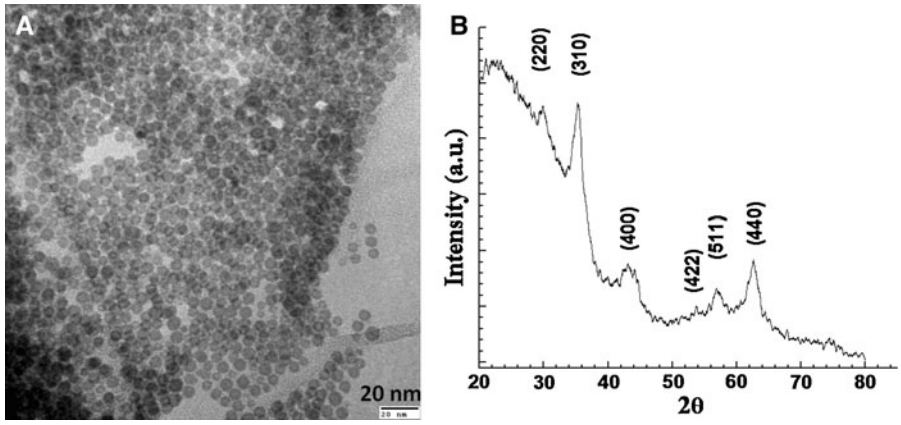

Fig. 1 **a** TEM image of the Fe_3O_4 nanoparticles used as nucleation seeds for the preparation of nickel phosphide nanorods and **b** XRD pattern of the Fe_3O_4 nanoparticles

average size and shape distribution were determined by counting nearly 300 particles per sample for statistical purposes, and it was found that the length of the nanorods varied from 13.2 ± 2.0 nm for 6 injections to 56.2 ± 17.1 nm for 15 injections. However, although the diameter of the nanorods was found to be almost identical to that of the seed nanoparticles, the nanorods became more polydispersed with an increase in the number of injections. Figure 3 shows the corresponding XRD patterns of these Ni_2P nanorods. The peak positions were entirely different from those of the nucleation seeds, and the patterns were assigned to the (111), (201), (210), (300), and (400) reflections of a hexagonal crystal structure (JCPDS Card No. 65-1989). The lattice parameters were calculated to be $a = 5.92$ Å and $c = 3.38$ Å, which were found to remain constant irrespective of the variations in the length of nanorods. The contribution of phosphorus in the Ni_2P nanorods was from TOP during the reaction. These results indicate that the synthesis of Ni_2P nanorods can be achieved by the addition of $Ni(acac)_2$–TOP mixture to the Fe_3O_4 seeds and the length of the nanorods could be manipulated by multiple injections of the precursor and the surfactant.

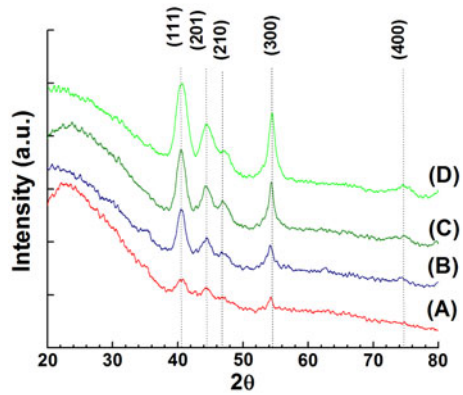

Fig. 3 XRD patterns of Ni_2P nanorods synthesized by (*A*) 6 injections, (*B*) 8 injections, (*C*) 12 injections, and (*D*) 15 injections of $Ni(acac)_2$–TOP to Fe_3O_4 seeds

It is noteworthy that in the case of Ni_2P nanorod synthesis, the change of the rod length was less sensitive to the number of injections as compared with

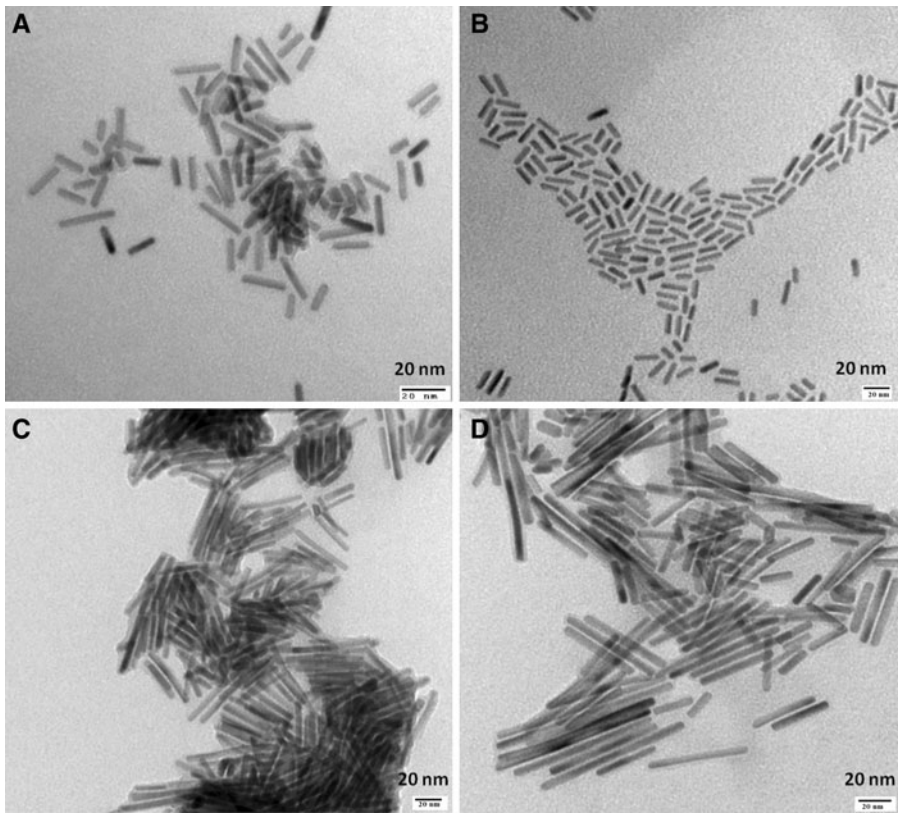

Fig. 2 TEM of Ni_2P nanorods synthesized by **a** 6 injections, **b** 8 injections, **c** 12 injections, and **d** 15 injections of $Ni(acac)_2$–TOP to Fe_3O_4 seeds

Fe_2P, where Fe_2P nanorods of 114.8 nm length were obtained after only 8 injections (Qian et al. 2004). This could be attributed to the greater stability of $Ni(acac)_2$–TOP in comparison to $Fe(CO)_5$–TOP, which led to slower growth of the Ni_2P nanorods.

We tried to synthesize Ni_2P nanorods by directly decomposing $Ni(acac)_2$–TOP without the use of Fe_3O_4 seeds. Although a clear change in color was observed indicating the decomposition of $Ni(acac)_2$–TOP, nanorods were not formed. As we are extending the findings of our previous research (Lo and Kuo 2010), we prepared Fe_2P nanorods in the mixture of TOPO tethered Fe_3O_4 nanoparticles, TOP, and DDAB. The controlled synthesis of the size of Fe_2P nanorods relies on the cooperative effects from the different binding capability of those surfactants. Different surfactant tethered seed particles would cause the complexity of reaction and this is beyond the scope of this work. In addition, the amount of Fe_3O_4 nanoparticles to prepare Ni_2P nanorods appeared to have no significant effect on the paramagnetic behavior of Ni_2P nanorods, as evident from the magnetic measurements of Ni_2P nanorods that will be discussed in the later section. This justifies the use of the iron oxide nanoparticles as nucleation seeds for the synthesis of the Ni_2P nanorods.

In our previous study, we found that the use of DDAB was necessary to form rod-shaped nanoparticles (Lo and Kuo 2010). Here, we further studied the role of DDAB in rod formation by varying its amount in total reaction mixture while keeping other parameters at a constant level. When we synthesized Ni_2P nanorods without the use of DDAB, there was a clear change in color in the reaction mixture due to the decomposition of $Ni(acac)_2$–TOP. However, no rod formation was observed. Figure 4 shows TEM images of the Ni_2P nanorods synthesized by using (a) 0.15 g, (b) 0.50 g, (c) 0.75 g, and (d) 1.0 g DDAB for 8 injections of Ni–TOP. It is evident from the Fig. 4a that when the DDAB quantity was small, not all the seed particles grew to form nanorods. When 0.50 g DDAB was used, a uniform growth of nanorods was observed and the nanorods were more monodispersed with the diameter similar to that of the seed particles (Fig. 4b). However, when the amount of DDAB was increased to 0.75 g, nanorods became less monodispersed and their diameters were more diverse (Fig. 4c). The dispersity of the diameter and length of nanorods became more pronounced when 1.0 g DDAB was used (Fig. 4d). The above observation further justifies the argument that the cooperative interaction of two surfactants, TOP and DDAB, enables the development of rod-shaped nanoparticles and an optimum DDAB quantity is necessary for getting uniform sized nanorods.

We further prepared $(Fe_xNi_y)_2P$ nanorods of different compositions. Figure 5 shows the TEM of $(Fe_xNi_y)_2P$ nanorods synthesized by 6 simultaneous injections of $Fe(CO)_5$–TOP and $Ni(acac)_2$–TOP to the Fe_3O_4 seeds for which the detailed experimental conditions are shown in Table 2. As evident from the images, nanorods of average lengths of 48.8 ± 11.2, 38.1 ± 3.4, and 21.1 ± 2.9 nm were obtained for $(Fe_{0.90}Ni_{0.10})_2P$, $(Fe_{0.80}Ni_{0.20})_2P$, and $(Fe_{0.75}Ni_{0.25})_2P$. The rod length decreased with an increase in the fraction of nickel in $(Fe_xNi_y)_2P$, which is again due to a more stable nature of $Ni(acac)_2$–TOP in comparison to $Fe(CO)_5$–TOP. Similar observations were reported by Yoon et al. where they prepared $(Fe_xNi_y)_2P$ nanorods with a single surfactant and found that with higher nickel content longer reaction time was required to synthesize nanorods for a particular length (Yoon et al. 2008). It should be noted that when Yoon et al. (2008) prepared bimetallic nanorods by multiple injections of metal phosphine mixtures without a syringe pump, a polydispersed mixture of spherical nanoparticles and nanorods was obtained. In our work, even without using a syringe pump, we successfully synthesized well-isolated nanorods with a greater degree of monodispersity. Thus, the presence of two surfactants eliminates the use of a syringe pump for getting nanorods by multiple injection procedure.

We also studied the effect of variations in the number of injections of $Ni(acac)_2$–TOP and $Fe(CO)_5$–TOP on the morphology and properties of $(Fe_xNi_y)_2P$ nanorods. The detailed experimental procedures are shown in Table 3. Figure 6 shows TEM of the $(Fe_{0.80}Ni_{0.20})_2P$ nanorods synthesized by 6 injections (Fig. 6a), 8 injections (Fig. 6b), and 12 injections (Fig. 6c) of $Fe(CO)_5$–TOP and $Ni(acac)_2$–TOP. In the case of 6-injection sample, the length of the $(Fe_{0.80}Ni_{0.20})_2P$ nanorods was found to be 38.1 ± 3.4 nm, while it was 53.4 ± 8.3 and 98.3 ± 20.5 nm, respectively, for 8- and 12-injection samples. These results are similar to that observed in the case of the Ni_2P nanorods where, with a fixed amount of metal precursor concentration, the length of nanorods increased with an increase in the number of injections of metal precursors. Figure 7 shows the XRD patterns of

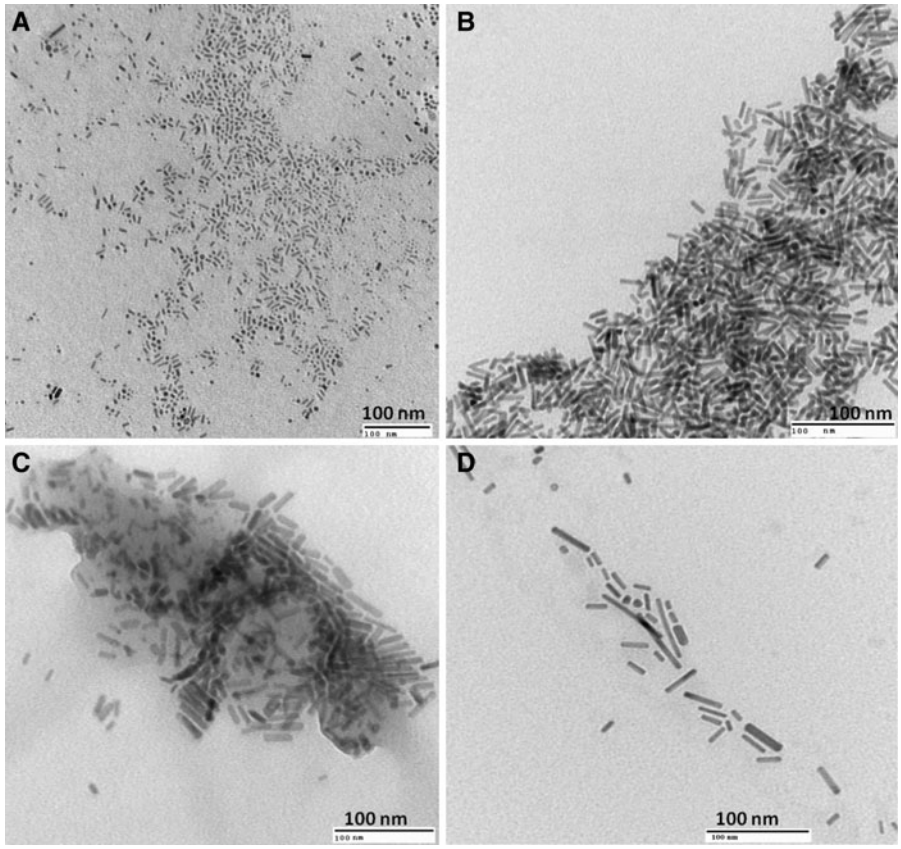

Fig. 4 TEM of Ni_2P nanorods synthesized by using **a** 0.15 g, **b** 0.50 g, **c** 0.75 g, and **d** 1.0 g DDAB for 8 injections of $Ni(acac)_2$–TOP to Fe_3O_4 seeds

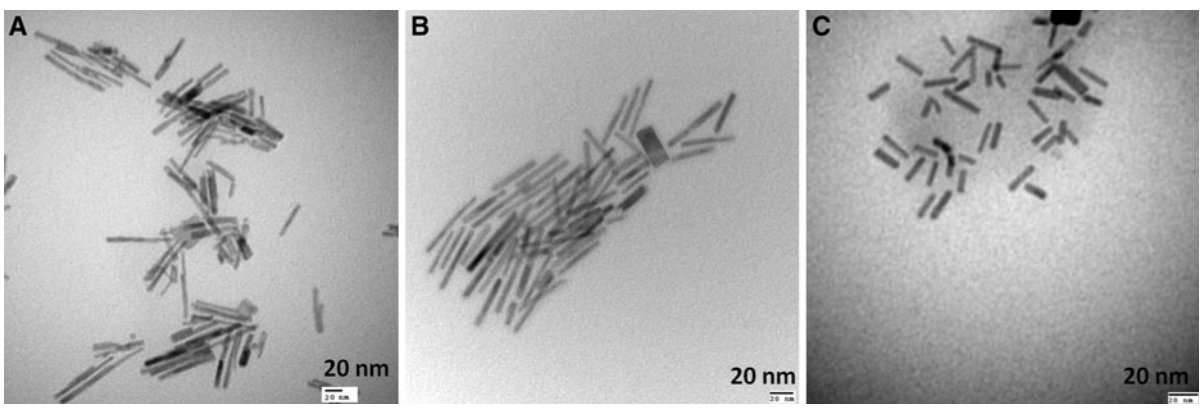

Fig. 5 TEM of **a** $(Fe_{0.90}Ni_{0.10})_2P$ nanorods, **b** $(Fe_{0.80}Ni_{0.20})_2P$ nanorods, and **c** $(Fe_{0.75}Ni_{0.25})_2P$ nanorods synthesized by 6 simultaneous injections of $Fe(CO)_5$–TOP and $Ni(acac)_2$–TOP mixtures to Fe_3O_4 seeds

Fe(Ni) concentration-dependent $(Fe_xNi_y)_2P$ nanorods (Fe = 0.75, 0.8, and 0.9) using 6 injections. We also add XRD of Ni_2P and Fe_2P into Fig. 7 in order to follow the structural evolution of $(Fe_xNi_y)_2P$ with x, in the form of nanorods. Our XRD shows that Ni_2P and Fe_2P nanorods share crystallographic features of (111), (210), and (300), in a fair agreement with the bulk case. These crystallographic similarities remain in the three $(Fe_xNi_y)_2P$ samples, pointing that the hexagonal structure is conserved in the bimetallic compounds, and thus their

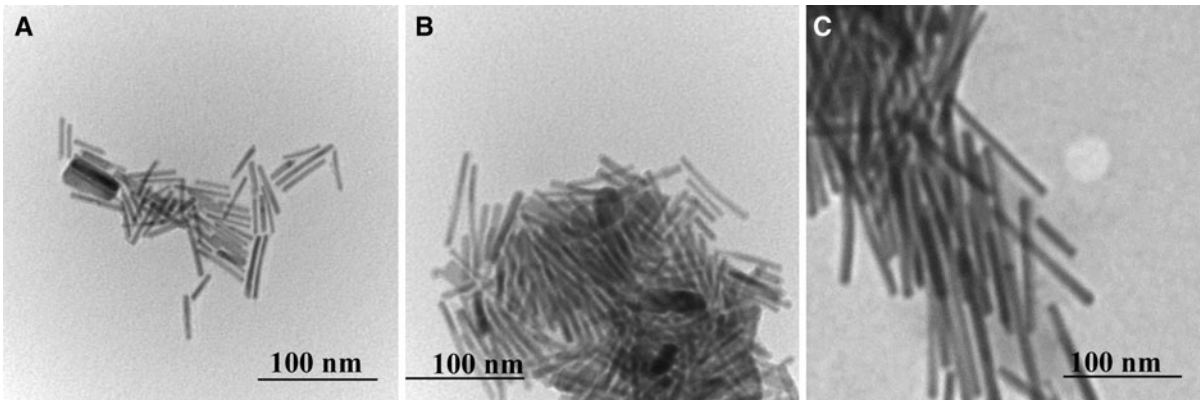

Fig. 6 TEM of $(Fe_{0.80}Ni_{0.20})_2P$ nanorods synthesized by **a** 6 injections, **b** 8 injections, and **c** 12 injections of $Fe(CO)_5$–TOP and $Ni(acac)_2$–TOP mixtures to Fe_3O_4 seeds

microstructural pictures can be thought of as a homogeneous solid-solution where Ni is atomically substituted by Fe. However, compared to their bulk forms, the deviation in (111) diffraction angle is almost undetectable for Ni_2P and Fe_2P nanorods, mainly due to the nature of poor crystallographic orderings. However, a shift in (111) toward a lower angle is still seeable in $(Fe_{0.75}Ni_{0.25})_2P$ as comparing with Ni_2P. For $(Fe_{0.75}Ni_{0.25})_2P$, its local lattice distortion on the (111) closely packed plane is expected to be strong with large Fe substitution, thus shifting (111) to a lower angle as the picture we observed in the bulk case. Nevertheless, the deviation almost disappears in $(Fe_{0.9}Ni_{0.1})_2P$, which can be explained as the relaxation of (111) from the dominance of Fe_2P.

In the following paragraphs, we discussed the magnetic properties of the Ni_2P and $(Fe_xNi_y)_2P$ nanorods. Figure 8 shows the temperature-dependent magnetizations of the Ni_2P nanorods synthesized by varying the number of injections of $Ni(acac)_2$–TOP. All the Ni_2P nanorods exhibited nearly identical ZFC and FC curves, which were distinct from the Fe_3O_4 nucleation seed, as the latter having a size-dimension of $\sim$5 nm in diameter usually exhibited superparamagnetic behaviors featuring significant irreversibility between ZFC and FC (Cattaruzza et al. 2005). This indicates that a different magnetic state emerged from within the nucleation seed as the injection of $Ni(acac)_2$–TOP was applied. The temperature-dependent magnetizations of the Ni_2P are consistent with literature (Park et al. 2005) and can be fitted by Curie–Weiss law, as highlighted in Fig. 9. The fitted Curie–Weiss

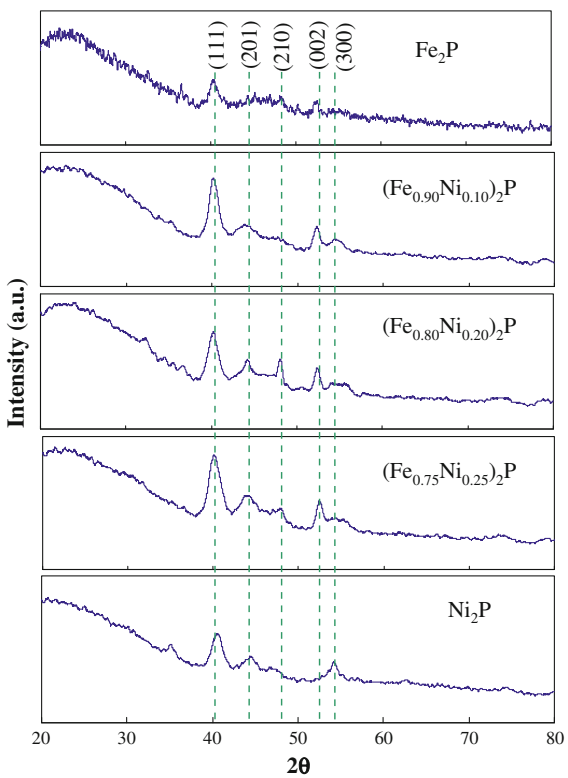

Fig. 7 XRD patterns of $(Fe_xNi_y)_2P$ nanorods with different compositions synthesized by 6 simultaneous injections of $Fe(CO)_5$–TOP and $Ni(acac)_2$–TOP mixtures to Fe_3O_4 seeds. The XRD patterns of Fe_2P and Ni_2P are also included as references

temperature (~ -357 K) is in close proximity to -364 K reported by Park et al. (2005) on a pure Ni_2P, suggesting that the Ni_2P phase was dominant to the

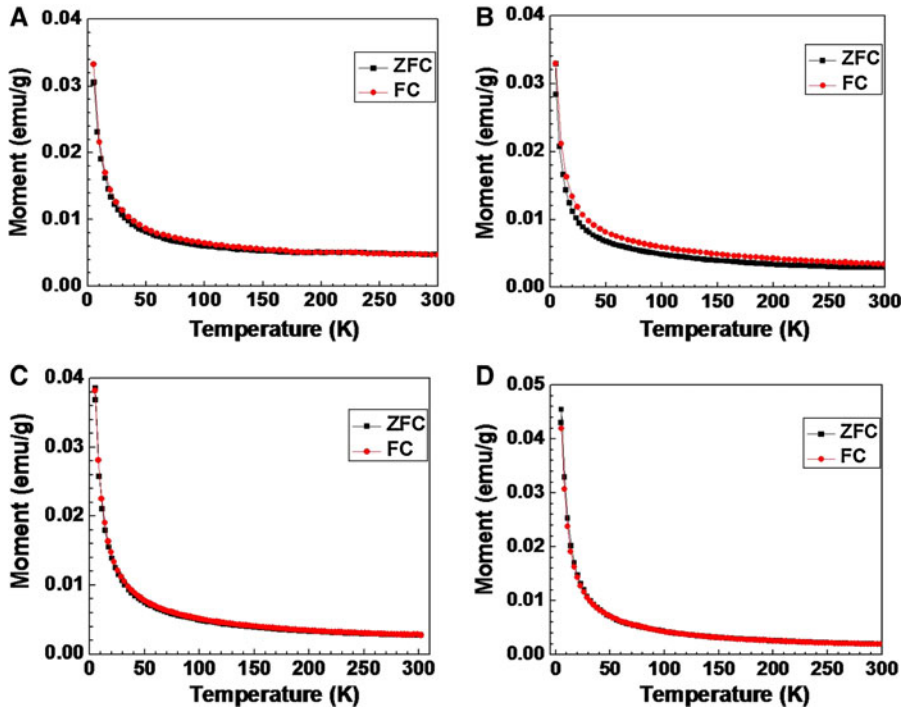

Fig. 8 Temperature-dependent magnetizations of Ni_2P nanorods synthesized by **a** 6 injections; **b** 8 injections; **c** 12 injections; and **d** 15 injections of $Ni(acac)_2$–TOP to Fe_3O_4 seeds

Fe_3O_4 and it dominated the magneto-structural phase of the rod in our case. The obtained Curie–Weiss behavior confirmed the paramagnetic phase of the Ni_2P, whereas the existence of an internal interaction between the localized moments cannot be neglected. Such behavior was only observed when the Ni_2P was shaped by nanostructure because its bulk counterpart was found to behave as a Pauli paramagnet whose magnetic susceptibility is independent of temperature (Fujii et al. 1988).

Figure 10 shows the temperature-dependent magnetizations of the $(Fe_xNi_y)_2P$ nanorods by 6 simultaneous injections of $Fe(CO)_5$–TOP and $Ni(acac)_2$–TOP. Unlike the Ni_2P, all the $(Fe_xNi_y)_2P$ nanorods displayed measureable blocking temperature (T_B) on ZFC, which is indicative of a superparamagnetic phase. For $(Fe_{0.90}Ni_{0.10})_2P$, its T_B (34 K) is comparable to Yoon's report on a pure Fe_2P ($\sim$76 K) (Yoon et al. 2008). Interestingly, the T_B gradually decreased with an increase in Ni content and almost disappeared in $(Fe_{0.75}Ni_{0.25})_2P$. For $(Fe_{0.75}Ni_{0.25})_2P$, its ZFC–FC irreversibility was largely reduced and the ZFC–FC curves underwent a similar trend as that of the Ni_2P (Fig. 8); namely, a fast decrease in moment upon warming. These results suggest a possible superparamagnetic $\rightarrow$ paramagnetic transition upon the increase of Ni content in the $(Fe_xNi_y)_2P$ nanorods. This conclusion is fairly supported by the M–H curves shown in Fig. 11 at which the measurements were conducted at 10 K. For $(Fe_{0.90}Ni_{0.10})_2P$, it displayed a clear ferromagnetic hysteresis curve with large saturation magnetization because of a restoration of the ferromagnetic state from the superparamagnetic state upon cooling. However, when a semi-paramagnetic phase was present as the case of $(Fe_{0.75}Ni_{0.25})_2P$, such ferromagnetic restoration was less significant, and the M–H curve was of less hysteresis together with reduced saturation magnetization. As pointed out by Sredniawa et al. (2000), bulk $(Fe_xNi_y)_2P$ exhibits ferromagnetic properties and a transition from ferromagnetic to paramagnetic behavior is obtained for $(Fe_xNi_y)_2P$ with high Ni contents. Meanwhile, the saturation magnetization of bulk $(Fe_xNi_y)_2P$ reduces almost linearly with an increase in Ni content (Zach et al. 2004). These literature results show good consistency with our experimental findings, suggesting that the magnetic response of the mixed phases of nanoparticles behaves similarly to the bulk materials.

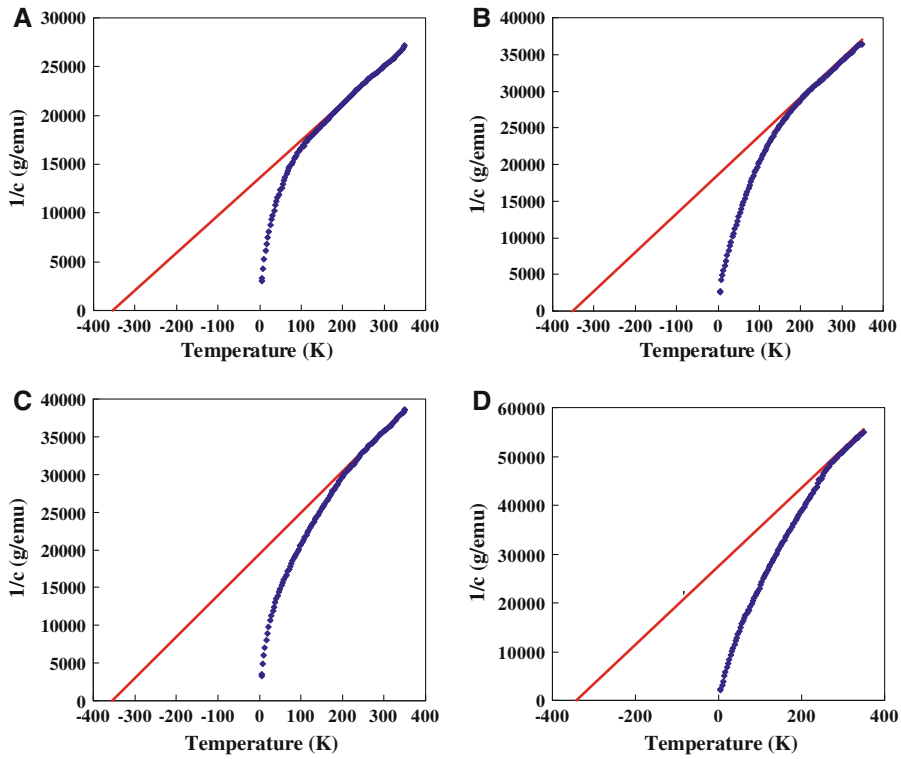

Fig. 9 Inverse magnetic susceptibilities of **a** 6 injections, **b** 8 injections, **c** 12 injections, and **d** 15 injections of $Ni(acac)_2$–TOP to Fe_3O_4 seeds

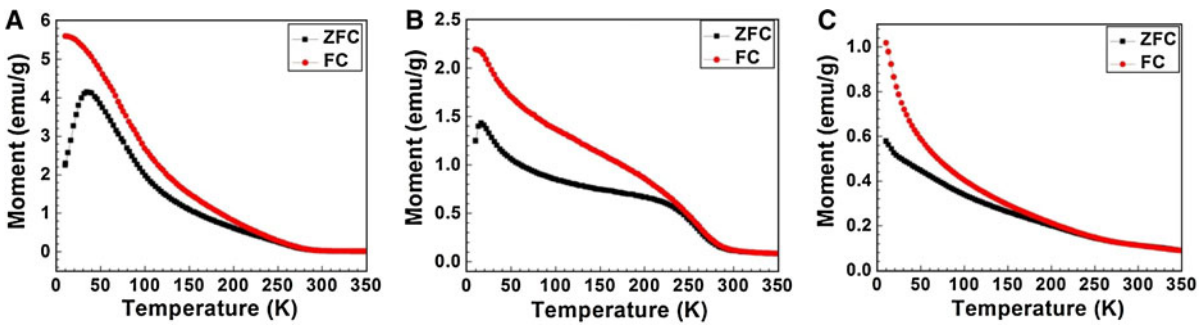

Fig. 10 Temperature-dependent magnetizations of **a** $(Fe_{0.90}Ni_{0.10})_2P$ nanorods, **b** $(Fe_{0.80}Ni_{0.20})_2P$ nanorods, and **c** $(Fe_{0.75}Ni_{0.25})_2P$ nanorods synthesized by 6 simultaneous injections of $Fe(CO)_5$–TOP and $Ni(acac)_2$–TOP mixtures to Fe_3O_4 seeds

Conclusions

We synthesized Ni_2P and bimetallic $(Fe_xNi_y)_2P$ nanorods by multiple injections of $Ni(acac)_2$–TOP and $Fe(CO)_5$–TOP mixtures in a preheated mixture of Fe_3O_4 nanoparticles, TOP, and DDAB. The Fe_3O_4 nanoparticles served as nucleation seeds, TOP as phosphorous source as well as a surfactant, and DDAB as a co-surfactant. The size of the nanorods could be varied by changing the number of injections of precursor metal–TOP at a constant total precursor concentration and a constant reaction time. The role of DDAB in the synthesis procedure was also studied. It was found that DDAB was necessary for the formation

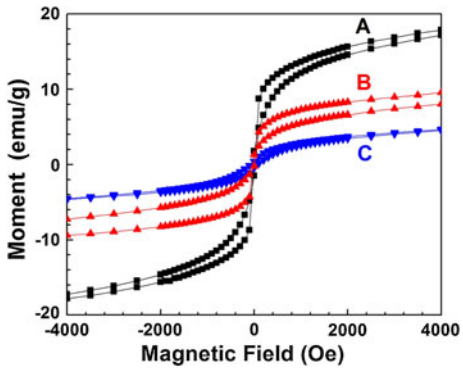

Fig. 11 M–H curves of *A* $(Fe_{0.90}Ni_{0.10})_2P$ nanorods, *B* $(Fe_{0.80}Ni_{0.20})_2P$ nanorods, and *C* $(Fe_{0.75}Ni_{0.25})_2P$ nanorods synthesized by 6 simultaneous injections of $Fe(CO)_5$–TOP and $Ni(acac)_2$–TOP mixtures to Fe_3O_4 seeds. Data were all taken at 10 K

of the nanorods and the variation in the DDAB quantity affected the monodispersity of the nanorods. Finally, the magnetic characterizations showed that the two kinds of nanorods exhibited different magnetic phases. The Ni_2P nanorods can be described as a paramagnet with a Curie–Weiss temperature of ~ -357 K. On the other hand, the $(Fe_xNi_y)_2P$ nanorods exhibited superparamagnetic characteristics and their magnetic states depend on the Ni content. We believe that our accomplishments on the synthesis of the Ni_2P and $(Fe_xNi_y)_2P$ nanorods in a controlled manner can be a mirror of the synthesis of phosphide nanorods with other metals.

Acknowledgments This work is financially supported by the Department of Engineering at National Cheng Kung University in Taiwan, the Department of Materials Science and Engineering at National Chiao Tung University in Taiwan, and the National Science Council with Grant no. NSC 98-2221-E-006-004-MY2 and NSC 98-2112-M-009-022-MY3.

References

Bai J, Takahoshi H, Ito H, Saito H, Wei F, Yang Z, Ishio S (2004) Coercivity map of perpendicular patterned CoCrPt medium investigated by using MFM. Phys Status Solidi A 201:1662–1665

Bieger T (1997) Fabrication, metallographic and tribologic investigations of LIGA-microstructures made of nickel phosphorous alloys. Microsyst Technol 3:155–163

Boyanov S, Bernardi J, Gillot F, Dupont L, Womes M, Tarascon JM, Monconduit L, Doublet ML (2006) FeP: another attractive anode for the Li-ion battery enlisting a reversible two-step insertion/conversion process. Chem Mater 18:3531–3538

Brock SL, Perera SC, Stamm L (2004) Chemical routes for production of transition-metal phosphides on the nanoscale: implications for advanced magnetic and catalytic materials. Chem Eur J 10:3364–3371

Cattaruzza F, Fiorani D, Flamini A, Imperatori P, Scavia G, Suber L, Testa AM, Mezzi A, Ausanio G, Plunkett WR (2005) Magnetite nanoparticles anchored to crystalline silicon surfaces. Chem Mater 17:3311–3316

Chubykalo-Fesenko OA, Chantrell RW (2004) Numerical evaluation of energy barriers and magnetic relaxation in interacting nanostructured magnetic systems. Phys B 343:189–194

Fujii S, Ishida S, Asano S (1988) Electronic structures and magnetic properties of Fe_2P, Co_2P and CoMnP. J Phys F 18:971–980

Gregg KA, Perera SC, Laws G, Shinozaki S, Brock SL (2006) Controlled synthesis of MnP nanorods: effect of shape anisotropy on magnetization. Chem Mater 18:879–886

Guan J, Wang Y, Qin M, Yang Y, Li X, Wang A (2009) Synthesis of transition-metal phosphides from oxidic precursors by reduction in hydrogen plasma. J Solid State Chem 182:1550–1555

Hou HW, Yang Q, Tan CR, Ji GB, Xie Y (2004) One-pot solution-phase synthesis of paramagnetic Co_2P nanorods. Chem Lett 33:1272–1273

Kelly AT, Rusakova I, Ould-Ely T, Hofmann C, Luttge A, Whitmire KH (2007) Iron phosphide nanostructures produced from a single-source organometallic precursor: nanorods, bundles, crosses, and spherulites. Nano Lett 7:2920–2925

Lee KB, Park S, Mirkin CA (2004) Multicomponent magnetic nanorods for biomolecular separations. Angew Chem Int Ed 116:3110–3112

Liu JW, Chen XY, Shao MW, An CH, Yu WC, Qian YT (2003) Surfactant-aided solvothermal synthesis of dinickel phosphide nanocrystallites using red phosphorus as starting materials. J Cryst Growth 252:297–301

Liu C, Chung SH, Jin Q, Sutton A, Yan F, Hoffmann A, Kay BK, Bader SD, Makowski L, Chen L (2006) Magnetic viruses via nano-capsid templates. J Magn Magn Mater 302:47–51

Lo CT, Kuo PY (2010) Synthesis and magnetic properties of iron phosphide nanorods. J Phys Chem C 114:4808–4815

Lukehart CM, Milne SB, Stock SR (1998) Formation of crystalline nanoclusters of Fe_2P, RuP, Co_2P, Rh_2P, Ni_2P, Pd_5P_2, or PtP_2 in a silica xerogel matrix from single-source molecular precursors. Chem Mater 10:903–908

Motojima S, Katsuhiko H, Takahashi Y, Sugiyama K (1979) Chemical vapor deposition of nickel phosphide Ni_2P. J Less Common Met 64:101–106

Motojima S, Wakamatsu T, Sugiyama K (1981) Corrosion stability of vapor-deposited transition metal phosphides at high temperature. J Less Common Met 82:379–383

Muthuswamy E, Kharel PR, Lawes G, Brock SL (2009) Control of phase in phosphide nanoparticles produced by metal nanoparticle transformation: Fe_2P and FeP. ACS Nano 3:2383–2393

Oyama ST (2003) Novel catalysts for advanced hydroprocessing: transition metal phosphides. J Catal 216:343–352

Park SJ, Kim S, Lee S, Khim ZG, Char K, Hyeon T (2000) Synthesis and magnetic studies of uniform iron nanorods and nanospheres. J Am Chem Soc 122:8581–8582

Park J, Koo B, Hwang Y, Bae C, An K, Park JG, Park HM, Hyeon T (2004) Novel synthesis of magnetic Fe_2P nanorods from thermal decomposition of continuously delivered precursors using a syringe pump. Angew Chem Int Ed 43:282–2285

Park J, Koo B, Hwang Y, Bae C, An K, Park JG, Park HM, Hyeon T (2005) Generalized synthesis of metal phosphide nanorods via thermal decomposition of continuously delivered metal–phosphine complexes using a syringe pump. J Am Chem Soc 127:8433–8440

Peng X, Wickham J, Alivisatos AP (1998) Kinetics of II–VI and III–V colloidal semiconductor nanocrystal growth: "focusing" of size distributions. J Am Chem Soc 120:5343–5344

Qian XF, Zhang XM, Wang C, Wang WZ, Qian YT (1998) A new way to prepare nanocrystalline dinickel phosphide. Mater Res Bull 33:669–672

Qian C, Kim F, Ma L, Tsui F, Yang P, Liu J (2004) Solution-phase synthesis of single-crystalline iron phosphide nanorods/nanowires. J Am Chem Soc 126:1195–1198

Sawhill SJ, Phillips DC, Bussell ME (2003) Thiophene hydrodesulfurization over supported nickel phosphide catalysts. J Catal 215:208–219

Senevirathne K, Burns AW, Bussell ME, Brock SL (2007) Synthesis and characterization of discrete nickel phosphide nanoparticles: effect of surface ligation chemistry on catalytic hydrodesulfurization of thiophene. Adv Funct Mater 17:3933–3939

Sredniawa B, Duraj R, Pacyna A, Bombik A, Zach R, Bacmann M, Fruchart D, Niziol S, Fornal P, Stanek J (2000) Magnetoelastic phase transitions and critical behaviour of $(Fe_{1-x}Ni_x)_2P$ system. Acta Phys Pol A 97:921–926

van Schnering HG, Honle W (1994) Encyclopedia of inorganic chemistry, vol 6. Wiley, Chichester 3106

Wang R, Smith KJ (2010) The effect of preparation conditions on the properties of high-surface area Ni_2P catalysts. App Catal A 380:149–164

Wang X, Clark P, Oyama ST (2002) Synthesis, characterization, and hydrotreating activity of several iron group transition metal phosphides. J Catal 208:321–331

Wang A, Qin M, Guan J, Wang L, Guo H, Li X, Wang Y, Prins R, Hu Y (2008) The synthesis of metal phosphides: reduction of oxide precursors in a hydrogen plasma. Angew Chem Int Ed 47:6052–6054

Wang JL, Yang Q, Zhang ZD, Sun SH (2010a) Phase-controlled synthesis of transition-metal phosphide nanowires by Ullmann-type reactions. Chem Eur J 16:7916–7924

Wang JL, Yang Q, Zhou J, Sun KW, Zhang ZD, Feng XM, Li TW (2010b) Magnetic Fe_2P nanowires and Fe_2P@C core@shell nanocables. Nano Res 3:211–221

Xie SH, Qiao MH, Zhou WZ, Luo G, He HY, Fan KN, Zhao TJ, Yuan WK (2005) Controlled synthesis, characterization, and crystallization of Ni–P nanospheres. J Phys Chem B 109:24361–24368

Yoon KY, Jang Y, Park J, Hwang Y, Koo B, Park JG, Hyeon T (2008) Synthesis of uniform-sized bimetallic iron-nickel phosphide nanorods. J Solid State Chem 181:1609–1613

Yunle G, Fan G, Qian Y, Huagui Z, Ziping Y (2002) A solvothermal synthesis of ultra-fine iron phosphide. Mater Res Bull 37:1101–1105

Zach R, Tobola J, Sredniawa B, Kaprzyk S, Casado C, Bacmann M, Fruchart D (2004) Magneto-elastic properties and electronic structure analysis of the $(Fe_{1-x}Ni_x)_2P$ system. J Alloy Compd 383:322–327

Zhang XF, Zhang QM, Zhao AQ, Guan J, He DM, Hu HQ, Liang CH (2010) Naphthalene hydrogenation over silica supported nickel phosphide in the absence and presence of *n*-containing compounds. Energy Fuels 24:3796–3803